Observation of Herzberg−Teller-type Wave Packet Motion in Porphyrin J-Aggregates Studied by Sub-5-fs Spectroscopy†

Hideaki Kano,‡ Takashi Saito, and Takayoshi Kobayashi*

Department of Physics, University of Tokyo, Hongo 7-3-1, Bunkyo, Tokyo 113-0033, Japan

Received: July 2, 2001; In Final Form: September 27, 2001

An interaction of the Frenkel exciton with the molecular vibration has been studied using sub-5-fs multichannel real-time spectroscopy. The coherent molecular vibration with a 135 ± 4 fs period is observed in the time-frequency two-dimensional difference absorption spectrum. An analysis of the phase and amplitude of the oscillation has revealed that both of the negative (bleaching and photoinduced emission) and positive (photoinduced absorption) signals are modulated synchronously. The experimental result is well explained in terms of a transition dipole moment modulated by a dynamic intensity borrowing from an intense B transition to a weak Q transition through the vibronic interaction. The wave packet observed in the present study can be classified as a Herzberg−Teller type in contrast with the frequently studied conventional Franck−Condon type.

1. Introduction

Femtosecond real-time spectroscopy has revealed a wealth of information about vibrational dynamics and coherence in molecular and condensed matter systems. A wave packet is prepared as a simultaneous excitation of vibrational manifold by an ultrashort laser pulse and is observed by several techniques such as time-resolved absorption and fluorescence spectroscopies. From a technological viewpoint, recent development of ultrafast science enables us to utilize an extremely short pulses in a sub-5-fs time scale.[1] Especially, noncollinearly phase-matched optical parametric conversion has been attracting a great interest as a novel method of ultrashort pulse generation with frequency tunability.[1−6] The noncollinear optical parametric amplifiers (NOPAs) based on this scheme have been exploited to generate sub-5-fs pulses in the visible by our group.[6] Such an ultrashort laser pulse can be applied to a study of the electron−vibration or exciton−phonon interaction through the observation of the vibrational wave packet. Since the first observation of molecular vibrations in the condensed phase by Rosker et al.,[7] coherent nuclear motions on the femtosecond time scale have been observed in dye molecules,[8,9] in polymers,[10,11] and in biological substances.[12−14] Concerning exciton systems, our group has also reported the coherent molecular vibration in polydiacetylene[11] and metal−halogen complex[15] which shows large lattice relaxation energy. On the other hand, in the case of the exciton system which couples weakly with the molecular vibration, few investigations have been performed,[13,14] and the origin of the oscillations has not been fully understood. Especially, the phase of the oscillations has not been investigated in detail.

In the present study, we apply the multichannel sub-5-fs real-time spectroscopy to molecular J-aggregates in order to shed light on the exciton−vibration coupling in the one-dimensional Frenkel exciton system, which shows small exciton−vibration interaction manifested by small Stokes shift of the fluorescence. Porphyrin J-aggregate is employed for the sample as one of model substances for Frenkel exciton system. Despite the weak exciton−vibration coupling, the coherent molecular vibration is clearly observed in the time dependence of the induced absorption change. Although we have already reported such transient oscillation in the same system,[16] the spectral range was restricted because of the monochromatic lock-in detection. In the present study, however, the induced absorption change was measured as a continuous spectrum. The direct observation of the transient oscillation and clear spectral dependence of the amplitude and phase enable us to elucidate the interaction between the exciton and the molecular vibration in more detail.

2. Experimental Section

2.1. Sub-5-fs Real-Time Pump−Probe Experimental Apparatus. The experimental setups of the sub-5-fs pulse generation[6] and sub-5-fs real-time spectroscopy[16] are described elsewhere. In the present study, multichannel pump−probe spectroscopy was employed with use of a CCD camera with a polychromator. The reference and probe pulses were dispersed by a polychromator (Acton, 320i; 150 groove/mm, 500 nm Blaze) and grabbed simultaneously by a two-dimensional-CCD camera (Roper Scientific, TE/CCD-1100-PB/UVAR; 1100 × 330 pixels) within 500 ms. The spectral resolution of the total system was about 4 nm. Two sets of 500 laser shots were accumulated under excited and nonexcited conditions one after the other, and this procedure was repeated 10 times for each delay-time. The broad spectrum of the probe pulse enabled the investigation over the wide spectral range from 1.6 to 2.3 eV. All measurements were performed at room temperature.

2.2. Sample Preparation and Stationary Absorption Spectrum. Tetraphenylporphine tetrasulfonic acid (TPPS; Tokyo Kasei) and poly(vinyl alcohol) (PVA; Kanto Chemical) were used without further purification. A sample preparation of a unidirectionally oriented film was described elsewhere.[16,17] Figure 1 shows stationary absorption spectrum of the J-aggregates and the laser spectrum. The absorption spectrum of the J-aggregate is characterized by mainly two bands, the

† Part of the special issue "Mitsuo Tasumi Festschrift".

* To whom correspondence should be addressed. Tel: +81−3−5841−4228. Fax: +81−3−5841−4240. E-mail: kobayashi@phys.s.u-tokyo.ac.jp.

‡ Present address: Department of Chemistry, University of Tokyo, Hongo 7-3-1, Bunkyo, Tokyo 113-0033, Japan.

10.1021/jp012493f CCC: $22.00 © 2002 American Chemical Society
Published on Web 11/20/2001

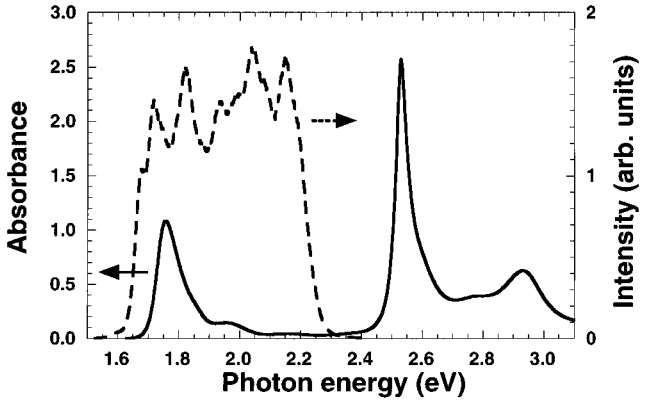

Figure 1. Stationary absorption spectrum of the TPPS J-aggregates (solid line) and laser spectrum (dashed line).

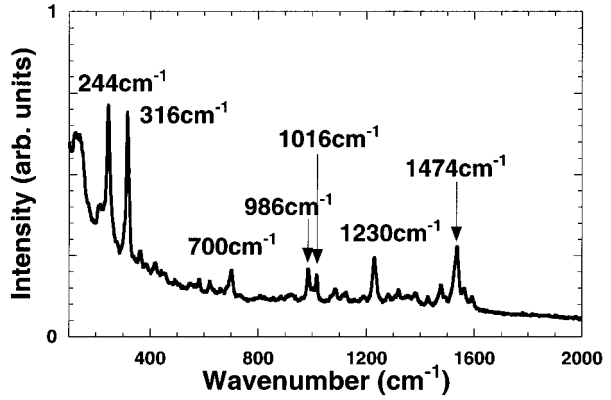

Figure 2. Resonance Raman spectrum of TPPS J-aggregates. The excitation wavelength is 488 nm.

B band (S_2-exciton state; $\hbar\omega_{max} = 2.53$ eV) and the Q band (S_1-exciton state; $\hbar\omega_{max} = 1.75$ eV); therefore, in the following, we shall focus on these two bands (quasi-two-band Frenkel-exciton system[16,18]).

2.3. Stationary Raman Spectrum. Figure 2 shows the resonance Raman spectrum of the sample under the excitation of the B band (2.53 eV). Two peaks are clearly observed at 244 and 316 cm^{-1}. These peaks have also been detected by Ohno et al.[19] and Akins et al.[20] They have reported that the two bands at 241 and 317 cm^{-1} are attributed to out-of-plane ruffling and doming modes, respectively.[20,21] They have also found that these two bands are drastically enhanced by a factor of more than 30 with respect to the corresponding two bands of diacid monomer at 233 and 310 cm^{-1}. Similar enhancement effect is also observed at 236 and 314 cm^{-1} of $TCPPH_42+$ (tetraphenylporphine tetracarboxyl acid) aggregates[20] and at 386 cm^{-1} of CuTOOPP ((5,10,15,20-tetrakis[4-(1-octyloxy)phenyl]-porphinato)copper-(II)) aggregates;[22] therefore, the enhancement is likely due to the aggregate formation. Because the aggregation formation is expected to influence the out-of-plane mode between adjacent porphinato macrocycles, the intermolecular interaction may also have to be taken into account.

3. Results

3.1. Real-Time Spectrum. Figure 3 shows three-dimensional plot of the time-resolved difference absorption spectrum, which clearly indicates the coherent oscillation as well as the slow-dynamics component. As shown in Figure 1, the laser spectrum covers the whole width of the S_1-exciton state of the TPPS J-aggregates, whereas the S_2-exciton state is outside of the laser spectrum. The S_2 exciton is not photoexcited in the excitation

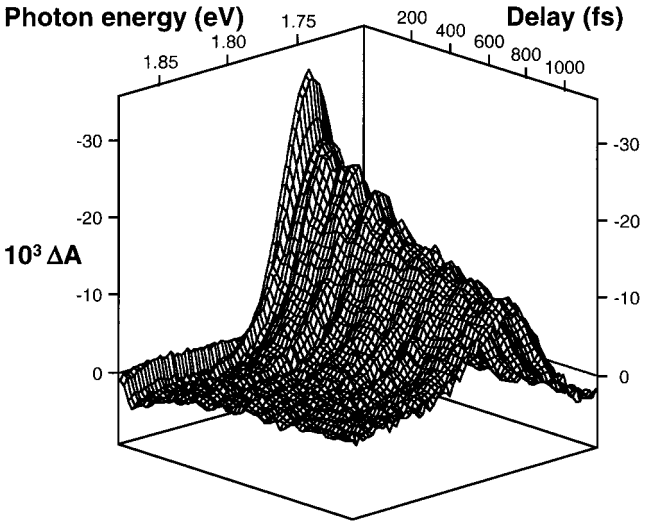

Figure 3. Three-dimensional plot of the time-resolved difference absorption spectrum of TPPS J-aggregates as functions of probe−photon energy and delay time. Data have been smoothened within 50 fs in order to clearly show the transient oscillation.

photon flux ($I = 1.2 \times 10^{29}$ photons/s cm^2) by the two-photon absorption process for the following reason. A typical value of the two-photon absorption cross section for anthracene is on the order of $10^{-50} cm^4$ s,[23] which is known to be relatively large among aromatic molecules. Even if the two-photon absorption cross section for the porphyrin J-aggregate, $\sigma^{(2)}$, is assumed to have a similar large value, the amount of $\sigma^{(2)}I = 1.2 \times 10^{-21}$ cm^2 is still much smaller than the one-photon absorption cross section for the porphyrin J-aggregate ($\sim 10^{-15}$ cm^2). Hence, no S_2 exciton can be created at the present experimental condition.

The difference absorption spectrum is displayed as a function of the delay time in Figure 4a. The predominant feature commonly appearing in the traces is high-frequency oscillations in addition to the underlying slow-dynamics transient components. The oscillatory signal size is drastically reduced around 1.78 eV. The overall slow dynamics of the induced change of the absorbance (ΔA) by photoexcitation originates from the excited states of excitons. Following the excitation of the J-aggregates, the negative ΔA is observed over the whole range of delay times for 1.71 eV $\leq E_{prob} \leq$1.78 eV, where E_{prob} represents the probe−photon energy. This is attributed to BL and PIE of the S_1-exciton state. At probe energies higher than 1.78 eV, the ΔA signal becomes positive due to the PIA. In fact, because of the BL around 1.85 eV, the ΔA signal overshoots to be negative around 1.80 eV as the delay time increases. The positive ΔA signal is more clearly observed if only the red side of the Q band is photoexcited. Note that the BL, PIE, and PIA spectra overlap with each other.

Measured decay traces are fitted to convoluted curves of the system response function with the following equation, and the results are presented in Figure 4a as dashed (A), dotted (B), and solid (ΔA) lines:

$$\Delta A(\hbar\omega) = A(\hbar\omega)\exp(-t/\tau) + B(\hbar\omega) \qquad (1)$$

The decay-time constant does not change significantly around the Q band and is determined to be about 320 fs. The spectral profile of each component ($A(\hbar\omega)$ solid and $B(\hbar\omega)$ dashed) is shown in Figure 5. In the following, the exponentially decaying component, $A(\hbar\omega)$, is referred to as a 320 fs decay component.

Next the origins of the 320 fs decay and constant components are to be discussed. The 320 fs decay component cannot be

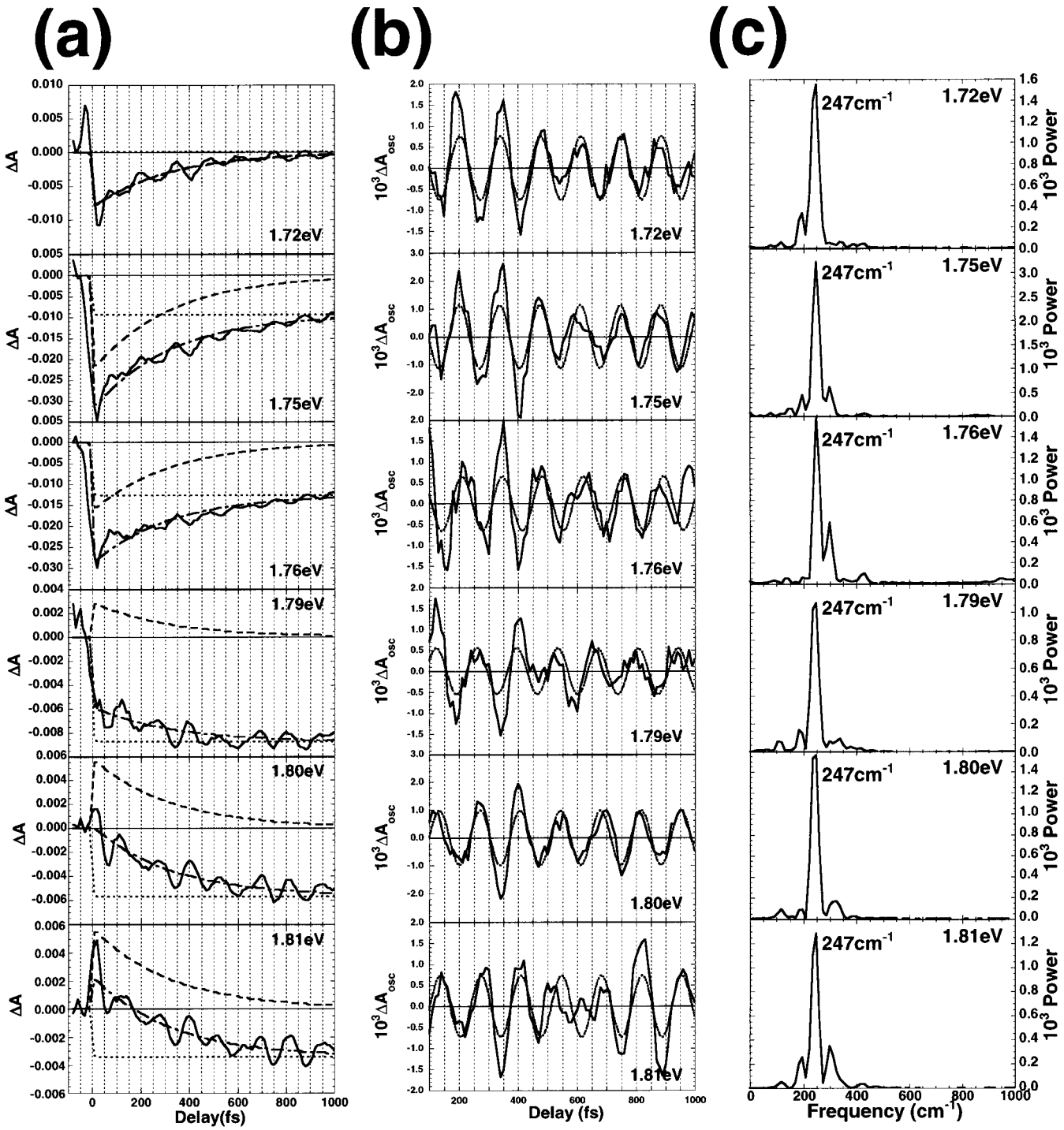

Figure 4. (a) Delay-time dependence of the induced absorption change of TPPS J-aggregates (solid line) and fitted results (dashed, dotted, and dot−dashed lines) at six probe−photon energies marked on the right; (b) Delay-time dependence of the oscillating component in a (solid line) and fitted result (dotted line); (c) Fourier-power spectrum of the oscillating component in b integrated from 100 fs to 1.2 ps.

attributed to the Q-exciton (S_1-exciton) lifetime, because its lifetime has been reported to be about 100−300 ps.[20] Because no B exciton (S_2 exciton) is created in the present condition, it cannot be ascribed to the B-exciton lifetime. The key is the blue-shifted PIA dominantly contributing to the 320 fs decay component, which is one of the characteristic features of the exciton system in the J-aggregates. Because of the Pauli exclusion principle (in other words, phase-space-filling effect in the present system), a creation of the exciton in the aggregate requires higher photon energy as the number of the exciton is increased.[18] Hence, the blue-shifted PIA is attributed to the transition to the multiexciton state [MES; $|n+1,S_1\rangle \leftarrow |n,S_1\rangle$ ($n = 1, 2, ...$)], and the 320 fs decay component is attributed to the fast relaxation process from higher MESs [$|n,S_1\rangle$ ($n = 2, 3, ...$)] to the one-exciton state, which is expected to be faster than the decay of the S_1 exciton. A similar decay-time constant (200 fs) has also been observed in the PIC J-aggregates and is also ascribed to the relaxation process from the higher MES.[24] On the other hand, the constant component can be explained by several relaxation in the Q band and the lifetime of the Q exciton.

3.2. Dynamics of Excitonic States. The time dependent ΔA signal consists of the slow relaxation component due to exciton decay and the highly oscillating component due to molecular

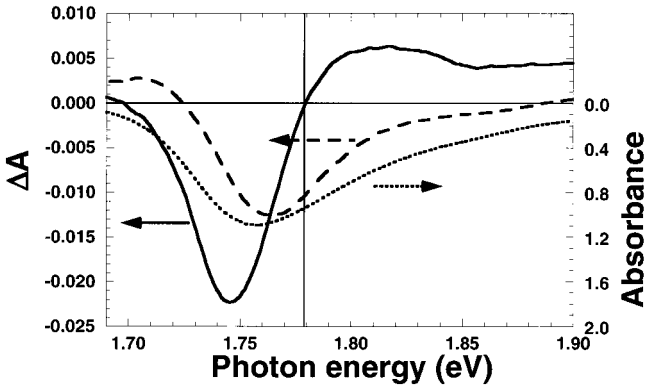

Figure 5. 320 fs decay (solid line) and constant (dashed line) components in the transient signal and the stationary absorption spectrum (dotted line).

vibration. It is noteworthy that the latter is observed only around the Q band. In this subsection, the slow relaxation component is to be discussed in detail. The excitonic transitions are classified into the following three components, namely, BL and PIE due to $|1,S_1\rangle \leftarrow |G\rangle$ and $|1,S_1\rangle \rightarrow |G\rangle$, respectively, and PIA due to the transition to the MES $[|n+1,S_1\rangle \leftarrow |n,S_1\rangle$ ($n = 1, 2, ...$)]. Here n in $|n,S_1\rangle$ denotes the number of the S_1 excitons (Q excitons) in a single aggregate. Because of the small Stokes shift, the BL is indistinguishable from PIE. Both of the BL and PIE give the negative signal in the induced absorption spectrum. On the other hand, the positive signal at the probe−photon energy slightly higher than the peak of the Q band originates from the PIA due to the transition such as $|n+1,S_1\rangle \leftarrow |n,S_1\rangle$ ($n = 1, 2, ...$). This PIA becomes remarkably observable when the red side of the Q band is excited. Because the transient oscillation is observed only around the Q band, the signals due to PIA as well as BL/PIE are modulated. In addition to that, another PIA due to the transition to higher-excited-exciton states $[|1,S_m\rangle \leftarrow |1,S_1\rangle$ ($m = 2, 3, ...$)] is also observed far above the Q band ($E_{prob} \gg 1.75$ eV) and around $E_{prob} < 1.71$ eV. Here, $|1,S_m\rangle$ indicates one-exciton state of S_m exciton, namely, the excited state of an exciton originated from an S_m-excited state in a TPPS molecule. It has been confirmed by 100 fs pump−probe spectroscopy.[25] This PIA does not show the transient oscillation.

3.3. Analysis of Coherent Molecular Vibration. For the discussion of the molecular vibration, smoothened traces by averaging over a 200 fs period are subtracted from the transient traces. We have carefully checked the dependence of the Fourier power spectrum of the time window (200 fs in the present report) and found that there was no prominent peak below 240 cm^{-1}. It has also been confirmed that the decay component is more dominant than the oscillating component below 240 cm^{-1} because a similar result to Figure 4c is obtained by the Fourier transformation of the oscillating component calculated by subtraction of the fitted slow-relaxation component from the trace (not shown). The two-dimensional contour plot of the Fourier-power spectrum of the oscillating components is also displayed in Figure 6 as functions of probe−photon energy and oscillation frequency. The resolution is determined to be 13 cm^{-1} (fwhm) by the width of the delay-time window in the Fourier transformation analysis. The Fourier spectrum clearly shows an intense peak at 247 ± 7 cm^{-1}. This frequency corresponds to an oscillation period of about 135 fs. Other higher modes are much weaker than the 247 cm^{-1} peak in the Fourier power spectrum. The peak around 247 cm^{-1} is observed in the resonance Raman spectrum shown in Figure 2, and it is assigned to the ruffling mode.[20] As is clearly shown in Figure 6, the

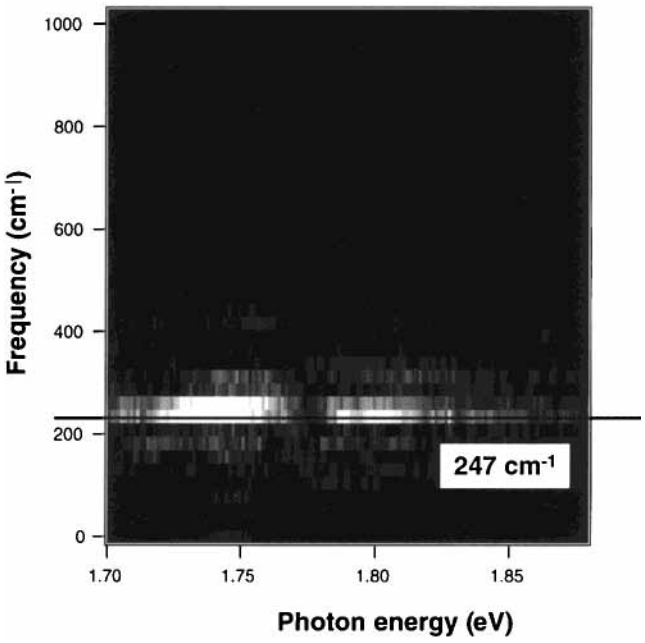

Figure 6. Two-dimensional contour plot of the Fourier power spectrum of the oscillating component of the induced absorption spectrum. The vertical and horizontal axes correspond to the probe−photon energy and oscillation frequency, respectively. Brighter regions indicate greater signal intensities.

intensity at the 247 cm^{-1} peak is drastically reduced at probe−photon energy around 1.78 eV, across which the sign of the oscillation amplitude is reversed (in other words, π-phase difference).

Figure 2 shows another peak at 316 cm^{-1} under the resonant excitation of the B band. This is assigned to the doming mode[20] and is also enhanced by aggregation. The peak around 315 cm^{-1} in Figure 4c can be attributed to the mode; however, it is very weak in the real-time spectrum in comparison with the ruffling mode. It may be explained by different coupling property of the B exciton with the Q excition for the doming mode. As will be discussed in a forthcoming paper, the real-time spectroscopy of the B excitation shows both of ruffling and doming modes.[26] In the following, the coherent oscillation with the frequency of 247 cm^{-1} will be considered.

3.4. Analysis of Phase and Amplitude of Oscillation. Owing to the extremely high time resolution, the phase and amplitude of the oscillation can be precisely evaluated. The oscillating component in Figure 4b is fitted to a cosine function with an fixed oscillating frequency of 247 cm^{-1}, which is also shown in Figure 4b. Figure 7 shows the probe−photon energy dependence of the phase and amplitude of the oscillation. The continuous spectra of the phase and amplitude clearly show that the phase is constant throughout the Q band ($(1.1 \pm 3.8) \times 10^{-1}$ radian) and that the sign of the amplitude is reversed around 1.78 eV. This result is consistent with the result calculated by the complex Fourier transformation. The probe−photon energy where the sign reversal takes place is slightly higher than the peak of the Q band and is located very close to the probe−photon energy of the null absorbance change in the 320 fs decay component. Because the sign of the BL/PIE signal is opposite to the sign of the PIA signal, the spectral profile of the amplitude indicates that the oscillations are in-phase for BL/PIE and PIA. This can be rephrased in the following way. All of the oscillations of the absolute value of absorbance change in the whole spectral range are synchronous with each other with a constant phase.

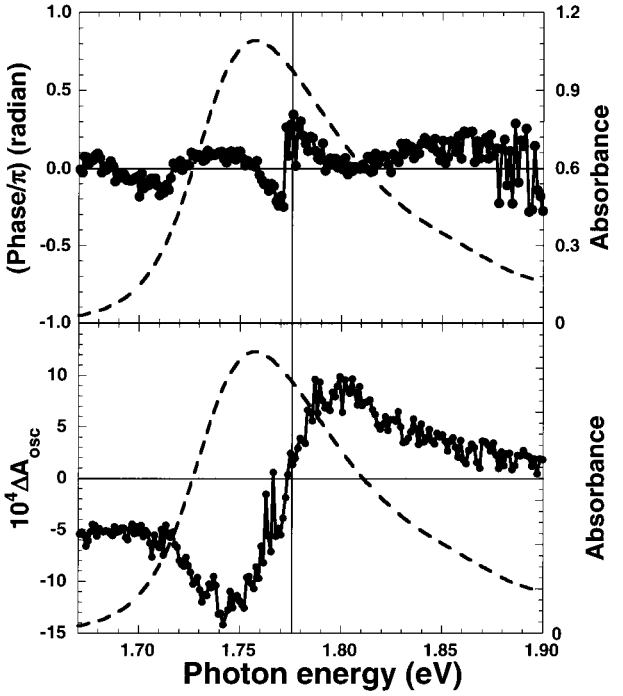

Figure 7. Probe−photon energy dependence of the phase (upper) and amplitude (lower) of the oscillation in the transient signals (dots). The oscillating component is fitted by a cosine function with a period of 135 fs.

4. Discussion

We are now in a position to investigate the exciton−vibration interaction in more detail. In comparison with the electron−vibration interaction in the monomer, the exciton−vibration interaction in the aggregate system is different in the following three aspects. First, the Stokes shift of the fluorescence is quite small (less than 20 meV). Second, as shown in Figure 2, the low-frequency Raman mode (244 and 316 cm^{-1}) is strongly enhanced. Last, the transition from the one-exciton state to the two-exciton state is located at the probe−photon energy slightly higher than the stationary absorption peak. Owing to these three differences, spectral and temporal profiles show characteristic properties inherent in the exciton system in the J-aggregates.

The experimental result shows the synchronous modulation in the transitions which are due to $|1,S_1\rangle \leftarrow |G\rangle$, $|1,S_1\rangle \rightarrow |G\rangle$, and $|n+1,S_1\rangle \leftarrow |n,S_1\rangle$ ($n = 1, 2, ...$). To interpret this intriguing experimental result, we shall examine following four models: (a) quantum beat between different *n*-exciton states, (b) conventional wave packet motion on the ground-state PES (in other words, impulsive stimulated Raman scattering; ISRS), (c) conventional wave packet motion on the excited-state PES, and (d) dynamic intensity borrowing (DIB)

4.1. Quantum Beat between Different Exciton States. First, model a is to be discussed. The transient oscillation could be ascribed to a beating between different *n*-exciton states (MESs; $n = 1, 2, ...$), which are simultaneously photoexcited by the broad excitation pulse. However, the oscillation persists longer than 1 ps, which is much longer than the relaxation time from the MESs to the one-exciton state (∼320 fs). Therefore, the quantum beat between the different *n*-exciton states is unlikely. In addition to that, the modulation frequency of 247 cm^{-1} is in excellent agreement with the resonance Raman spectrum. It indicates that the oscillation originates not from the inherent property of the exciton but from the exciton−vibration interaction. The quantum beat between the one-exciton states with different momenta ($k = 1, 3, ...$) could also be one of the candidates. However, model a can be ruled out because the oscillator strength is concentrated on $k = 1$ one-exciton state (∼80%), and other transition ($k = 3, 5, ...$) is expected to take place only with a vanishingly small probability.

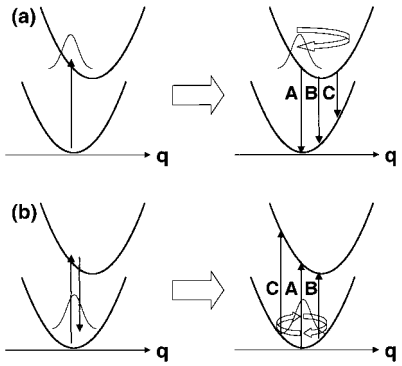

Figure 8. Wave packet motions on the (a) excited- and (b) ground-state PES. In the case of a, the phases of the oscillation are 0, $\pi/2$, and π for A, B, and C, respectively. On the other hand, in the case of b, the phases of the oscillation are 0, $\pi/2$, and $3\pi/2$ for A, B, and C, respectively.

4.2. Wave Packet Motion on Ground-State PES. Second, we shall focus on model b. The time dependence of the absorbance change due to the wave packet prepared on the ground-state PES (ISRS; Figure 8b) is described with a sine function, and the amplitude spectrum of the oscillation is approximately expressed by the first derivative of the stationary absorption spectrum. In the present condition, however, the contribution of the ground-state oscillation is negligible because of the following two reasons. First, the oscillation is not described by a sine function but is much closer to a cosine function. Second, the phase of the oscillation in the BL/PIE signal is identical with the one of the oscillation in the PIA, which must be ascribed to the wave packet motion on the excited-state PES. If the ground-state oscillation is also contributing to the signal, this excellent agreement of the phase relationship will be no longer observed. Therefore, the wave packet motion on the ground-state PES does not contribute much to the observed oscillatory signal. Similar conclusions have been drawn by Bradforth et al.[27] and Chachisvilis et al.[13] in biological systems.

4.3. Wave Packet Motion on Excited-State PES. Third, model c is to be considered. In this scheme, the wave packet prepared by the excitation pulse move on the excited-state PES as shown in Figure 8a; therefore, the oscillation amplitude is given by a cosine function. If the system consists of only the ground state and one excited state (two-level system), the amplitude spectrum of the oscillation can be approximately expressed by the first derivative of a fluorescence spectrum (strictly speaking, derivative of the spectrum of a hot luminescence). The phases of the oscillation are 0, $\pi/2$, and π for three probe−photon energies at A, B, and C, respectively, marked in Figure 8a. In the present experiment, the Stokes shift of the fluorescence signal is measured to be less than 20 meV; therefore, the whole probe−photon energy dependence of the phase shown in Figure 8a can be detected with use of our broadband laser pulse. Assuming a wave packet motion on a harmonic PES, the oscillation must show π-phase difference between $E_{probe} = E_{abs} = 1.76$ eV and $E_{probe} = 2E_{fluo} - E_{abs} = 1.72$ eV, where E_{abs} and E_{fluo} are the peak photon energies of the absorption and fluorescence spectra, respectively. The former and the latter correspond to the positions indicated as A and C, respectively, in Figure 8a. Although it can be resolved enough in the present condition, the π-phase difference is not observed

between 1.72 and 1.76 eV but found around 1.78 eV, which is slightly higher than $E_{abs} = 1.76$ eV. Hence, the oscillation cannot be explained only by taking account of the PIE process from the excited-state wave packet. In the present case, in fact, the PIA due to the transition to MES must also be considered. This PIA is located at the probe−photon energy slightly higher than the peak of the Q band. If the amplitude of the oscillation due to the PIA is more dominant than the one due to the BL/PIE, the above-mentioned π-phase difference may be canceled. However, it is not the case because of the following reason. As is discussed in ref 28, the oscillator strength of the transition due to PIA (mainly from the $k = 1$ one-exciton state to the $(k_1,k_2) = (2,1)$ two-exciton state; $1.27(N + 1)^2\mu_0^2$, where μ_0 is a transition dipole moment of the monomer) is 1.57 times larger than the oscillator strength of the transition due to BL (from the ground state to the $k = 1$ one-exciton state; $0.81(N + 1)^2\mu_0^2$).[28] On the other hand, to explain the phase spectrum of the oscillation component, the ratio of the PIA to PIE must be 1.95 ± 0.02, which is substantially larger than the theoretical estimation (1.57). In addition, there are two more remaining problems for model c. First, the conventional wave packet model (c) is based on the simultaneous photoexcitation of the multivibrational quantum states depending on the Franck−Condon factor. However, the vibronic excitation of the Q band is known to originate mainly from the Herzberg−Teller-type transition.[29] This will be discussed later in more detail. Second, if the signal originates from model c, the signal intensity integrated in whole spectral region of the Q band must not be modulated, because this model only produces the spectral shift. As will be shown later, however, the integrated signal intensity shows nonnegligible modulation, which cannot be explained by model c. Concerning the phase of the oscillation, Champion et al. have discussed the effect of the inhomogeneous broadening.[30] However, the phase spectrum was calculated based on the wavelength-selected pump pulse, and it does not correspond to our experimental condition (broadband excitation).

4.4. Dynamic Intensity Borrowing. In this subsection, a following new mechanism is proposed, which also induces the coherent oscillation and modulation of the transition dipole moment of the Q band. This model is beyond Condon approximation, because the transition dipole moment does depend on the normal vibrational coordinate. The modulation frequency corresponds to the 247 cm^{-1} ruffling-mode vibration. The key is the optical property of the Q band. Although the Q state is the originally forbidden state because of the symmetry of the electronic structure, it becomes allowed owing to the mixing of electronic property with the B state by the configuration interaction (electron−electron correlation) and vibronic coupling.[29,31] Therefore, the modulation of the Q transition can be explained by an additional intensity borrowing from the B band. We call this new mechanism "dynamic intensity borrowing (DIB)". Figure 9 shows a schematic energy diagram for the DIB mechanism. Because of the small Stokes shift of the stationary fluorescence spectrum, it is assumed that the bottom of the excited-state PES is simply located just above the bottom of the ground-state PES. A wave packet is created on the excited-state PES because of the vibronic coupling and a small anharmonicity. The wave packet on the excited-state PES becomes narrower or broader along with the time evolution, and no probe−photon energy dependence is expected as shown in Figure 8 unless the DIB occurs. The DIB allows the oscillator strength to be modulated as a function of the normal coordinate, which results in the coherent oscillation in the induced absorption signal as shown in Figure 10. The increase (or decrease)

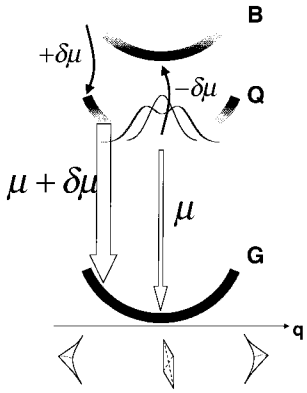

Figure 9. Energy diagram for the J-aggregates (model d). A simplified picture of the ruffling mode is also shown below. The larger and smaller oscillator strength is indicated as a thick line with partially dark and light parts of the PES of the Q and B band.

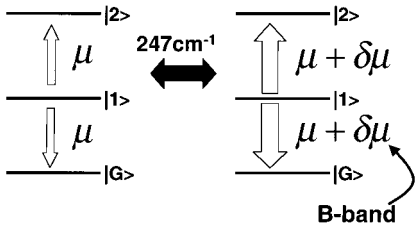

Figure 10. Modulated transition dipole moment due to the coherent molecular vibration (model d). $|G\rangle$, $|1\rangle$, and $|2\rangle$ denote the ground state and the one- and two-exciton states, respectively.

of the transition dipole moment is reflected by the increase (or decrease) of the signal intensity both of the BL/PIE and PIA. As a result, DIB can explain the synchronous oscillations for the BL/PIE and PIA in terms of the modulation of the transition dipole moment. If this model is valid, the total signal intensity associated with the Q exciton must also be modulated. It can be evaluated by integrating the signal intensity over the whole spectral region of the Q band, which is defined by $\int_{Qband} \Delta A(\hbar\omega)\, d\omega$. The integrated signal intensity from 1.65 to 1.91 eV is displayed in Figure 11 as a function of the delay time. It clearly shows the nonnegligible amplitude of the coherent oscillation mainly with a frequency of 247 cm^{-1}. Considering that the spectral range from 1.65 to 1.91 eV is wide enough to sum all nonnegligible oscillating signals due to the Q band, the oscillator strength of the Q exciton is also modulated by the 247 cm^{-1} frequency component. It cannot be explained by model c, because model c predicts only the spectral shift.

Similar intensity borrowing mechanism has also been discussed in the stationary resonance Raman spectrum of metalloporphyrins.[32−34] The resonance Raman spectrum under the B-band excitation shows dominant contribution of the Albrecht A term (Franck−Condon type).[35] On the other hand, in the case of the Q band, the scattering intensity from depolarized and anormalously polarized vibrations is often as intense as polarized mode scattering.[31] Concerning the Q-band excitation, the Albrecht B term (Herzberg−Teller type) scattering is dominated and is also explained by the vibronic intensity borrowing mechanism from the B band to the Q band.[33,34]

4.4.1. Theory for Herzberg−Teller-type Wave Packet Motion. According to model d, the modulation of the transition dipole moment depends on the normal coordinate. Hence, this model can also be called a "Herzberg−Teller-type" wave packet motion in comparison with the conventional "Franck−Condon-type" wave packet motion. In the following, we derive an

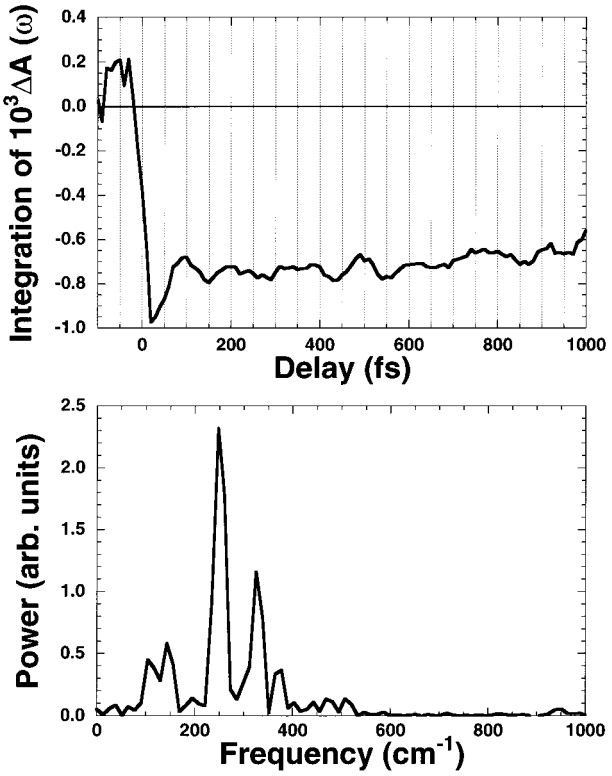

Figure 11. Integrated signal intensity of the induced absorption change from 1.65 to 1.91 eV (upper) and the Fourier power spectra of the oscillating component (lower).

analytical expression for the wave packet motion based on the coordinate-dependent transition dipole moment. In general, the vibronic coupling effect is approximately expressed by the expansion of the transition dipole moment, $\hat{\mu}(\hat{q})$, using Herzberg−Teller expansion of the ground- and excited-state wave functions. Here, $\hat{q}$ denotes the normal coordinate. In the present system, and the vibronic coupling occurs dominantly between the Q and B bands; therefore, the following three wave functions are considered:

$$|G(r,q)\rangle = |\psi_G(r)\chi_n^G(q)\rangle \tag{2}$$

$$|B(r,q)\rangle = \left(|\psi_B(r)\rangle - \frac{H_{vib}}{\Delta E_{BQ}} q|\psi_B(r)\rangle\right)|\chi_l^B(q)\rangle \tag{3}$$

$$|Q(r,q)\rangle = \left(|\psi_Q(r)\rangle + \frac{H_{vib}}{\Delta E_{BQ}} q|\psi_B(r)\rangle\right)|\chi_m^Q(q)\rangle \tag{4}$$

Here, $\psi_X(r)$ and $\chi^X(q)$ represent wave functions of the electron and nuclear for the X (= G, B, and Q) state, respectively, as a function of the electron and nuclear coordinates, r and q, respectively. In the nuclear wave functions, the vibrational quantum numbers are indicated as n, l, and m. The first term in $|Q(r,q)\rangle$, namely, $|\psi_Q(r)\rangle$, consists of two wave functions as follows:

$$|\psi_Q(r)\rangle = |\psi_Q^0(r)\rangle + \alpha|\psi_B(r)\rangle \tag{5}$$

The first term, $|\psi_Q^0(r)\rangle$, is an optically forbidden state. On the hand, the second term is an optically allowed state, which originates from the configuration interaction (CI) with the B band. An coefficient of α represents the degree of the CI. The matrix element of the transition dipole moment from the ground state to the Q band is calculated as follows:

$$\begin{aligned}\langle Q(r,q)|\hat{\mu}(\hat{q})|G(r,q)\rangle &= \left\langle \chi_m^Q(q)\left|\left(\langle\psi_Q(r)| + \frac{H_{vib}}{\Delta E_{BQ}}\langle\psi_B(r)|\hat{q}\right)\mu|\psi_G(r)\chi_n^G(q)\right\rangle\right. \\ &= \mu_{QG}\langle\chi_m^Q|\chi_n^G\rangle \cong |\alpha|^2\mu_{BG} \quad (\text{if } n = m = 0) \end{aligned} \tag{6}$$

$$= \beta\mu_{BG}q_{mn} \quad (\text{if } n \neq m \text{ and } m \neq 0) \tag{7}$$

Here, $\mu_{QG} = \langle\psi_Q|\mu|\psi_G\rangle$, $\mu_{BG} = \langle\psi_B|\mu|\psi_G\rangle$, $\beta = H_{vib}/\Delta E_{BQ}$, and $q_{mn} = \langle\chi_m^Q|\mu|\chi_n^G\rangle$. Although multimode effects should be taken into account,[36] we roughly assume $\langle\chi_0^Q|\chi_0^G\rangle \cong 1$, which means that all vibronic excitation is not caused by the Franck−Condon component but caused by the term in eq 7 associated with the vibronic coupling.[29] Although the symmetry is important for the vibronic interaction and the coefficient, q_{mn}, the symmetry of the ruffling mode for the aggregate is not as well defined as for the monomer. Taking account of the time evolution, the wave function, $|\Psi(t)\rangle$, is expressed as follows assuming an impulsive limit:

$$\begin{aligned}|\Psi(t)\rangle &\equiv \exp(-i\hat{H}t/\hbar)\hat{\mu}|G(r,q)\rangle \\ &\propto |\alpha|^2\mu_{BG}|\psi_B\chi_0^Q\rangle \\ &\quad + \beta\mu_{BG}\sum_{m\neq 0} q_{m0}\exp(-im\Omega t)|\psi_B\chi_m^Q\rangle \end{aligned} \tag{8}$$

Here, Ω corresponds to the 247 cm^{-1} vibrational frequency. The transition from the excited-state wave packet, $|\Psi(t)\rangle$, to the ground state, $|G(r,q)\rangle$, is calculated as follows using eq 8:

$$\begin{aligned}\langle G(r,q)|\mu|\Psi(t)\rangle &= |\alpha|^4(\mu_{BG})^4 \\ &\quad + |\beta|^2(\mu_{BG})^2\sum_{m\neq 0}|q_{m0}|^2\exp(-im\Omega t) \end{aligned} \tag{9}$$

Because the signal intensity of the absorbance change, ΔA, is proportional to the square of the eq 9, the wave packet can be created by the Q transition through the vibronic coupling with the B transition. As shown in eq 9, the DIB corresponds to a real-time observation of the vibronic coupling (vibronic intensity borrowing) between the Q and B bands, which is manifested by the coefficient of q_{m0}. In similar way, we can also calculate the oscillator strength of the transition from the n-exciton state to the $(n + 1)$-exciton state $[|n + 1,S_1\rangle \leftarrow |n,S_1\rangle\ (n = 1, 2, ...)]$. Therefore, both of the BL/PIE and PIA signals are synchronously modulated, which agree well with the experimental result.

4.4.2. Evaluation of the Amount of the Modulated Transition Dipole Moment. As is discussed, the Q and B transitions are mixed by the DIB, which is induced by the sub-5-fs excitation pulse through the vibrational motion of the porphyrin molecules composing a J-aggregate. On the basis of the DIB mechanism, the amount of the modulation of the transition dipole moment can be evaluated. The normalized modulation of the transition dipole moment is simply expressed as $\delta\mu_{QG}/\mu_{QG}$, in which μ_{QG} and $\delta\mu_{QG}$ represent the Q transition dipole moment of a TPPS molecule and a change of μ_{QG} induced by the molecular vibration, respectively. It is noted that the modulation of μ_{QG} also changes the intermolecular dipole−dipole interaction, J, to $J + \delta J$ which is given by

$$J_{QG} = \mu_{QG}{}^2(1 - 3\cos^2\theta)/\hbar a^3$$

$$\frac{\delta J_{QG}}{J_{QG}} = \frac{2\delta\mu_{QG}}{\mu_{QG}} + \frac{3\sin(2\theta)}{3\cos^2\theta - 1}\delta\theta - \frac{3}{a}\delta a \tag{10}$$

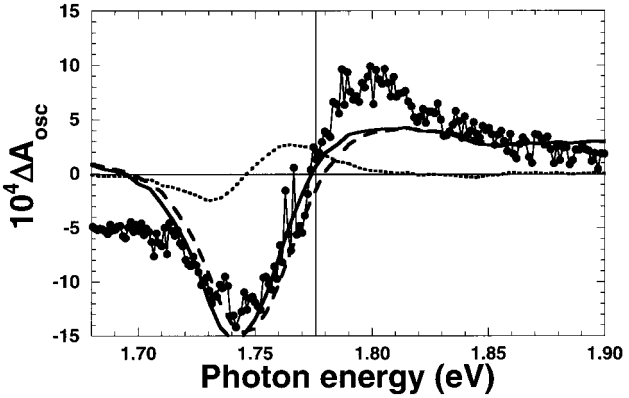

Figure 12. Fitted result based on model d; DIB.

where all transition dipoles in the molecules are assumed to be parallel and making an angle θ with the aggregate axis and the molecules are equidistant with a lattice constant a. Because the transition energy from the ground state to the lowest one-exciton state is originally red-shifted by $2J$ in comparison with the one of the monomer, the modulation of J gives rise to a peak shift of the J band in the transient absorption spectrum. This is one of the characteristic features of the exciton system in comparison with the molecular system. In what follows, the data are analyzed phenomenologically. The nonlinear spectrum, $S_{NL}(\omega)$, is assumed to be modulated as $S'_{NL}(\omega)$ by $\delta\mu_{QG}$ and $\delta(2J)$, which is given by

$$S'_{NL}(\omega) = S_{NL}(\omega - \delta\omega(t))(1 + \delta\alpha(t)), \tag{11}$$

where

$$\delta\alpha(t) = \delta\alpha \cos(\Omega t) \equiv \delta(\mu_{QG}^2)/\mu_{QG}^2 \cos(\Omega t), \tag{12}$$

$$\delta\omega(t) = \delta\omega \cos(\Omega t) \equiv \delta(2J) \cos(\Omega t) \tag{13}$$

Here, $\delta\alpha$ and $\delta\omega$ correspond to the amplitude modulation and the spectral shift of the nonlinear spectrum, respectively. The modulation frequency, Ω, corresponds to 247 cm^{-1} ruffling mode. In the present model, it is assumed that both $\delta\alpha$ and $\delta\omega$ are independent of the probe−photon energy, ω, and that all μ_{QG} and J are modulated effectively. Equation 11 is approximately expressed as

$$S'_{NL}(\omega) \approx S_{NL}(\omega) + \left(\delta\alpha S_{NL}(\omega) - \delta\omega \frac{dS_{NL}(\omega)}{d\omega}\right) \cos(\Omega t)$$
$$= S_{slow}(\omega) + S_{osc}(\omega) \cos(\Omega t). \tag{14}$$

The nonlinear spectrum, $S_{NL}(\omega)$, consists of the slow-dynamics component ($S_{slow}(\omega)$) and the oscillating component ($S_{osc}(\omega)$). For the slow-dynamics component, the 320 fs decay component is employed. Figure 12 shows the fitted results ($\delta\alpha S_{NL}(\omega)$ dashed, $\delta\omega$ $(dS_{NL}(\omega))/(d\omega)$ dotted, $S_{osc}(\omega)$ solid) for the oscillating component using eq 14. The experimental result is reproduced satisfactory by the fitted curve and $\delta\alpha = (6 \pm 1) \times 10^{-2}$ and $\delta\omega = (-8 \pm 4) \times 10^{-4}$eV are obtained. From the value of $\delta\alpha$, $\delta\mu_{QG}/\mu_{QG}$ is estimated to be $(3 \pm 1) \times 10^{-2}$. Using $\delta\alpha$, $\delta\omega$, and eq 10, the amount of the dipole−dipole interaction of the Q band ($2J_Q$) can be estimated to be $2J_Q = \delta\omega/\delta\alpha = (13 \pm 9)$ meV assuming $\delta\theta = \delta a = 0$. This value is much smaller than the one calculated by the energy shifts from the monomer to the J-aggregate in the stationary absorption spectrum (170 meV). This may mean that the energy shift in the stationary absorption spectrum is not only due to the dipole−dipole interaction. It is also supported by the fact that the amount of the energy shift for the B band is only about twice in comparison with the one for the Q band. Because the oscillator strength is 10 times different between them ($\mu_Q^2/\mu_B^2 = 0.1$), the ratio of J, namely, J_Q/J_B, must also be different in the same order (see eq 10). A Coulomb interaction between molecules caused by the aggregation could be one of the other mechanisms associated with this energy shift.

4.4.3. Evaluation of the Amount of the Oscillator Strength Transfer. On the basis of the vibronic coupling theory, we estimate the amount of the oscillator strength transfer from the B band to the Q band. The perturbed transition dipole moment of the Q band, μ'_{QG}, is expressed as follows:

$$\mu'_{QG} = \mu_{QG} + \delta\mu_{QG}$$
$$= \mu_{QG} + \frac{V_{DIB}}{\Delta E_{BQ}}\mu_{BG} \tag{15}$$

Here, V_{DIB} denotes the interaction Hamiltonian due to the DIB. Equation 15 is written as follows:

$$\frac{\delta\mu_{QG}}{\mu_{QG}} = \frac{V_{DIB}}{\Delta E_{BQ}}\frac{\mu_{BG}}{\mu_{QG}} \tag{16}$$

Here, $\Delta E_{BQ} \approx 0.94$ eV and $\mu_{QG}/\mu_{BG} \approx 0.32$ are estimated from the stationary absorption spectrum of the monomer. The amount of $\delta\mu_{QG}/\mu_{QG}$ has also been estimated to be 3%. Hence, $V_{DIB} = 9$ meV $= 73$ cm^{-1} is obtained using eq 16. This value, V_{DIB}, is much less than the vibration frequency, 247 cm^{-1}, which is consistent with our model. The modulated transition dipole moment is expressed as follows:

$$\mu'_{QG} = \mu_{QG} + \delta\mu_{QG} = (32 + 0.96) \times 10^{-2}\mu_{BG} \tag{17}$$

Consequently, the modulation of the Q-transition dipole moment in the real-time spectrum is estimated to be about 0.96% of the B-transition dipole moment, which is in good agreement with our previous report.[16]

5. Conclusion

The coherent molecular vibration coupled to the Frenkel exciton is observed using sub-5-fs laser pulses and multichannel pump−probe experimental setup. The oscillation originates from the molecular vibration and is assigned to the 247 cm^{-1} ruffling mode. In comparison with the conventional model (c) regarded as Franck−Condon-type wave packet motion (Figure 8a), the DIB (Figure 9; model d), which we propose for the first time, can be called Herzberg−Teller-type wave packet motion. In fact, the DIB corresponds to the real-time observation of the Herzberg−Teller-type wave packet motion. The coherent oscillation is explained by the modulated transition dipole moment of the Q transition, which is caused by the DIB mechanism from the intense B band to the weak Q band through the molecular vibration. The modulated transition dipole moment is estimated to be about 3%, which corresponds to about 0.96% borrowing of the B-transition dipole moment.

Acknowledgment. The authors thank Drs. H. F. Hofmann and T. Fuji for stimulating discussions. The authors are indebted to Dr. A. Shirakawa of University of Electro-communications for helpful advice. Thanks are due to Dr. Y. Takasu and Prof. I. Nishio of Aoyama Gauin University for Raman scattering measurements. The authors acknowledge Dr. S. Abe of Eletrotechnical Laboratory for fruitful discussion. The work is partly

supported by Research for the Future of Japan Society for the Promotion of Science (JSPS-RFTF-97P-00101).

References and Notes

(1) Kobayashi, T.; Shirakawa, A. *Appl. Phys. B* **2000**, *70*, S239.
(2) Gale, G. M.; Cavallari, M.; Driscoll, T. J.; Hasche, F. *Opt. Lett.* **1995**, *20*, 1562.
(3) Shirakawa, A.; Kobayashi, T. *Appl. Phys. Lett.* **1998**, *72*, 147.
(4) Cerullo, G.; Nisoli, M.; Silvestri, S. De. *Opt. Lett.* **1998**, *23*, 1283.
(5) Shirakawa, A.; Sakane, I.; Kobayashi, T. *Opt. Lett.* **1998**, *23*, 1292.
(6) Shirakawa, A.; Sakane, I.; Takasaka, M.; Kobayashi, T. *Appl. Phys. Lett.* **1999**, *74*, 2268.
(7) Rosker, M. J.; Wise, F. W.; Tang, C. L. *Phys. Rev. Lett.* **1986**, *57*, 321.
(8) Fragnito, H. L.; Bigot, J. Y.; Becker, P. C.; Shank, C. V. *Chem. Phys. Lett.* **1989**, *160*, 101.
(9) Pollard, W. T.; Dexheimer, S. L.; Wang, Q.; Peteanu, L. A.; Shank, C. V.; Mathies, R. A. *J. Phys. Chem.* **1992**, *96*, 6147.
(10) Cerullo, G.; Lanzani, G.; Muccini, M.; Taliani, C.; Silvestri, S. D. *Phys. Rev. Lett.* **1999**, *83*, 231.
(11) Kobayashi, T.; Shirakawa, A. *Chem. Phys. Lett.* **2000**, *321*, 385.
(12) Vos, M. H.; Rappaport, F.; Lambry, J. C.; Breton, J.; Martin, J. L. *Nature* **1993**, *363*, 320.
(13) Chachisvilis, M.; Sundstrom, V. *Chem. Phys. Lett.* **1996**, *261*, 165.
(14) Monshouwer, R.; Baltuska, A.; Mourik, F. V.; Grondelle, R. V. *J. Phys. Chem. A* **1998**, *102*, 4360.
(15) Sugita, A.; Saito, T.; Kano, H.; Yamashita, M.; Kobayashi, T. *Phys. Rev. Lett.* **2001**, *86*, 2158.
(16) Kano, H.; Saito, T.; Kobayashi, T. *J. Phys. Chem. B* **2001**, *105*, 413.
(17) Misawa, K.; Ono, H.; Minoshima, K.; Kobayashi, T. *Appl. Phys. Lett.* **1993**, *63*, 577.
(18) Knoester, J.; Spano, F. C. *Phys. Rev. Lett.* **1995**, *74*, 2780.
(19) Ohno, O.; Kaizu, Y.; Kobayashi, H. *J. Chem. Phys.* **1993**, *99*, 4128.
(20) Akins, D. L.; Ozcelik, S.; Zhu, H. R.; Guo, C. *J. Phys. Chem.* **1996**, *100*, 14390.
(21) Ren, B.; Tian, Z. Q.; Guo, C.; Akins, D. L. *Chem. Phys. Lett.* **2000**, *328*, 17.
(22) Shick, G. A.; O'Grady, M. R.; Tiwari, R. K. *J. Chem. Phys.* **1993**, *97*, 1339.
(23) Pantell, R.; Pradere, F.; Hanus, J.; Schott, M.; Pathoff, H. *J. Chem. Phys.* **1967**, *46*, 3507.
(24) Minoshima, K.; Taiji, M.; Misawa, K.; Kobayashi, T. *Chem. Phys. Lett.* **1994**, *218*, 67.
(25) Kano, H.; Kobayashi, T. *J. Chem. Phys.*, in press.
(26) Kano, H.; Kobayashi, T. Real-time spectroscopy of porphyrin J-aggregates by S_1- and S_2-exciton excitations. Manuscript in preparation.
(27) Bradforth, S. E.; Jimenez, R.; Mourik, F. V.; Grondelle, R. V.; Fleming, G. R. *J. Phys. Chem.* **1995**, *99*, 16179.
(28) Burgel, M.; Wiersma, D. A.; Duppen, K. *J. Chem. Phys.* **1995**, *102*, 20.
(29) Perrin, M. H.; Gouterman, M.; Perrin, C. L. *J. Chem. Phys.* **1969**, *50*, 4137.
(30) Kumer, A. T. N.; Rosca, F.; Widom, A.; Champion, P. M. *J. Chem. Phys.* **2001**, *114*, 701.
(31) Dolphin, D., Ed. *The Porphyrins, volume III, Physical Chemistry, Part A*; Academic Press: New York, 1979.
(32) Schelnutt, J. A. *J. Chem. Phys.* **1980**, *72*, 3948.
(33) Li, X.-Y.; Czernuszewicz, R. S.; Kincaid, J. R.; Spiro, T. G. *J. Am. Chem. Soc.* **1989**, *111*, 7012.
(34) Czernuszewicz, R. S.; Li, X.-Y.; Spiro, T. G. *J. Am. Chem. Soc.* **1989**, *111*, 7024.
(35) Albrecht, A. C. *J. Chem. Phys.* **1960**, *33*, 156.
(36) Champion, P. M. *Chem. Phys. Lett.* **1982**, *86*, 231.